metals

MDPI

Article

Influence of Oxygen and Zirconium Contents on the Mechanical Properties of Ti-23Nb-0.7Ta-Zr-O Alloys

Kunlun Si [1], Xu Wang [1], Zhaolong Yin [1], Yi Yang [1,*], Songquan Wu [1], Geping Li [2], Kai Zhang [1,3], Hao Wang [1] and Aijun Huang [3]

[1] School of Materials and Chemistry, University of Shanghai for Science and Technology, Shanghai 200093, China; sikunlun@163.com (K.S.); 18303408104@163.com (X.W.); velin2011679654@163.com (Z.Y.); sqwu@alum.imr.ac.cn (S.W.); kai.zhang@usst.edu.cn (K.Z.); haowang7@usst.edu.cn (H.W.)
[2] Institute of Metal Research, Chinese Academy of Sciences, Shenyang 110016, China; gpli@imr.ac.cn
[3] Department of Materials Science and Engineering, Monash University, Clayton, VIC 3800, Australia; aijun.huang@monash.edu
* Correspondence: yiyang.imr@163.com

Abstract: Ti-23Nb-0.7Ta-(0, 2)Zr-(1.2, 4, 6, 10)O alloys were prepared using a non-consumable arc-melting method. The tensile property of Ti-23Nb-0.7Ta-2Zr-1.2O alloys was tested at temperatures from −196 °C to 750 °C. The influence of O and Zr contents on thermal forgeability, room-temperature hardness and tensile property at 750 °C was investigated. For Ti-23Nb-0.7Ta-2Zr-1.2O alloy, the tensile strength decreased, and the ductility increased with the temperature increase. O and Zr had a negative effect on the thermal forgeability. Room-temperature hardness and tensile strength increased with an increase in O and Zr contents due to interstitial, solid solution strengthening and second-phase strengthening. All of the alloys exhibited high ductility at 750 °C with the total elongation above 34% and reductions in area above 80%.

Keywords: titanium alloy; element; mechanical property; microstructure

Citation: Si, K.; Wang, X.; Yin, Z.; Yang, Y.; Wu, S.; Li, G.; Zhang, K.; Wang, H.; Huang, A. Influence of Oxygen and Zirconium Contents on the Mechanical Properties of Ti-23Nb-0.7Ta-Zr-O Alloys. *Metals* **2022**, *12*, 1018. https://doi.org/10.3390/met12061018

Academic Editor: Carlos Garcia-Mateo

Received: 21 April 2022
Accepted: 6 June 2022
Published: 16 June 2022

1. Introduction

Because of their high specific strength, low Young's modulus, good corrosion resistance and superior biocompatibility, titanium alloys have been widely applied in various fields [1–6]. By controlling the composition and microstructures, the mechanical properties may vary within a wide range [7–12]. Zr is one of the most important elements in titanium alloys. It can strengthen α and β phases via solid solution strengthening and result in a higher strength [13–18]. In addition, in Ti-3Al-8V-6Cr-4Mo-xZr (x = 0, 2, 4 and 6 wt.%) alloys Zr and trace impurity Si may form $(TiZr)_6Si_3$ silicide to increase the strength via β grain refinement and precipitation strengthening [19]. The effects of Zr content on the mechanical properties of conventional titanium alloys were described as decreasing ductility and increasing strength at room and high temperatures [13,20]. Moreover, Zr can increase the stability of the β phase and be treated as a β stabilizer in β titanium alloys [18,21–23].

Some so-called "impurity" elements, such as N and O, could be added to titanium alloys as alloying elements to improve the mechanical properties, like Ti-22Nb-O (at.%, unless otherwise noted) [24], Ti-10V-2Fe-3V-N (wt.%) [25], Ti-30Nb-12Zr-O(N) (wt.%) [26], Ti-24Nb-4Zr-8Sn-O (wt.%) [27], Ti-35Nb-7Zr-5Ta-O (wt.%) [28,29] and Gum Metal [30]. As an interstitial element, even a small amount of N or O can change the properties dramatically. Additionally, too much N or O may damage the ductility of the alloy. Therefore, the concentrations of added N or O in the alloy are generally at a relatively low level.

Gum Metal [30] is one of the representative alloys containing Zr and O. It represents a group of multifunctional β titanium alloys, with the composition fundamentally expressed as Ti-24(Nb + Ta + V)-(Zr, Hf)-O. O concentration was restricted in the range

of 0.7–3.0 at.%. It has been reported that Zr and O might form Zr-O atom clusters to enhance the strengthening effect of Zr and O on each other [30]. Various alloy composition combinations are available, such as Ti-9Nb-12Ta-3V-6Zr-O, Ti-23Nb-0.7Ta-2Zr-O, Ti-20Nb-3.5Ta-3.4Zr-O, etc. [30–32]. Of which, Ti-23Nb-0.7Ta-2Zr-O alloy has received the most extensive attention, due to lower levels of Ta, an amazing complex deformation mode and superior properties [32–45]. Some works [31,33,46–49] have studied the effect of O content on the mechanical properties of the Ti-23Nb-0.7Ta-2Zr-O alloy. In the O content range of 0.3–3.0% the attainable elastic strain, elastic modulus and tensile strength increased, and ductility decreased as the O content increased.

All the above studies are about the mechanical properties at room or cryogenic temperatures. The effects of O and Zr contents on mechanical properties at relatively high temperatures, especially for Ti-23Nb-0.7Ta-Zr-O alloy with quite high O content, remain unknown.

In the present work, Ti-23Nb-0.7Ta-(0, 2)Zr-(1.2, 4, 6, 10)O alloys were prepared using a non-consumable arc-melting method. The influence of temperature on the tensile properties of Ti-23Nb-0.7Ta-2Zr-1.2O alloy, as well as the influence of O and Zr contents on thermal forgeability, room-temperature hardness and tensile property at 750 °C, were investigated.

2. Materials and Methods

The nominal compositions of the alloys are shown in Table 1. The measured composition of the 2Zr-1.2O alloy was Ti-22.4Nb-0.73Ta-2Zr-1.34O, which was very close to the nominal composition as shown in Table 1 [39,41]. The β transus of the alloys were calculated according to Sun's study [50] and presented in Table 1. Ti sponge, Zr sponge, pure Nb, Ta_2O_5 and TiO_2 were used as the raw materials. The alloys were melted three times using a KEJING MSM20-8 consumable arc-melting furnace (Shenyang Kejing Auto-Instrument Co., LTD, Shenyang, China) under argon protection. The melting current was 600 A and the magnetic stirring current was 15 A. The 2Zr-1.2O alloy ingot was 1300 g and the others were 60 g. 2Zr-1.2O alloy was open-forged at 1080 °C and then 750 °C, and other ingots were open-forged at 1220 °C. After forging, 2Zr-1.2O alloy was solutionized at 1010 °C for 30 min followed by water quenching, and then the alloy was compressed at room temperature to 77% reduction in height with a constant crosshead speed of 0.1 mm/s. (0, 2)Zr-4O, (0, 2)Zr-6O and (0, 2)Zr-10O alloys were solutionized at 900 °C, 950 °C and 1050 °C, respectively, for 1 h followed by furnace cooling.

Table 1. Nominal compositions of the studied alloys and the heat treatments. WQ-water quenching, FC-furnace cooling.

Alloy Name	Nominal Composition, at.%	Calculated β Transus, °C	Ingot Weight, g	Open Forging Temperature, °C	Post Treatment
2Zr-1.2O	Ti-23Nb-0.7Ta-2Zr-1.2O	574	1300	1080 and 750	1010 °C, 30 min, WQ, 77% compression
2Zr-4O	Ti-23Nb-0.7Ta-2Zr-4O	695	60	1220	900 °C, 1 h, FC
2Zr-6O	Ti-23Nb-0.7Ta-2Zr-6O	827	60	1220	950 °C, 1 h, FC
2Zr-10O	Ti-23Nb-0.7Ta-2Zr-10O	1234	60	1220	1050 °C, 1 h, FC
0Zr-4O	Ti-23Nb-0.7Ta-4O	707	60	1220	900 °C, 1 h, FC
0Zr-6O	Ti-23Nb-0.7Ta-6O	842	60	1220	950 °C, 1 h, FC
0Zr-10O	Ti-23Nb-0.7Ta-10O	1264	60	1220	1050 °C, 1 h, FC

Microstructure observations were performed by a ZEISS Axiovert 200 MAT optical microscope (Zeiss, Oberkochen, Germany) and a Hitachi S-3400N scanning electron microscope (SEM, Hitachi, Tokyo, Japan) under 30 KV. Tensile fracture surfaces were examined using Hitachi S-3400N SEM. A SHIMADZU EPMA-1610 electron probe microanalyzer (Shimadzu Corporation, Kyoto, Japan) was employed to obtain the distribution of elements. Phase identification was carried out with a Rigaku D/max-2400PC X-ray diffractometer (XRD) using Cu-Kα at 56 kV and a current 182 mA. Vickers-hardness (HV) was tested using a FUTURE FM-700e digital micro-hardness-testing device (FUTURE-TECH CORP.,

Kawasaki, Japan) with a load of 300 g and a dwell time of 15 s. Each specimen was tested five times. Uniaxial tensile test was carried out using a SHIMADZU AG-5000A machine (Shimadzu Corporation, Kyoto, Japan) at −196 °C with strain rates of 8.3×10^{-4}/s and 25×10^{-4}/s before and after yielding, respectively, and a SHIMADZU DCS-25T machine (Shimadzu Corporation, Kyoto, Japan) at 19 °C, 250 °C and 750 °C with strain rates of 2.5×10^{-4}/s and 12.5×10^{-4}/s before and after yielding, respectively. The elevated temperature tensile samples were heated to the testing temperature at a rate of 20 °C/min and held for 10 min in the air before tensile testing. The tensile specimens were cylindrical rods with a gauge diameter of 3 mm and a gauge length of 12 mm. One specimen was tested at each temperature. The strain gauges were used in the cryogenic and ambient temperature tensile tests until yielding. The elongation and reduction in area were measured after fracture.

3. Results

3.1. Effects of O and Zr on Thermal Forgeability

2Zr-1.2O alloy showed excellent thermal forgeability and compression plasticity even at room temperature as reported in our previous work [39,41]. The morphologies of a 60 g ingot and open-forged specimens are shown in Figure 1. The forged specimens were 10–13 mm square bars except for 2Zr-10O alloy because of its lower forgeability. Thermal forgeability of the alloys was judged from the surface cracks. It could be observed that three Zr-free specimens presented good surfaces, as shown in Figure 1e–g. For the specimens with 2% Zr the size of surface cracks increased as O content increased, as shown in Figure 1b–d. Especially, 2Zr-10O alloy cracked severely. It indicates that the thermal forgeability of the alloys decreased as O content increased with the addition of Zr.

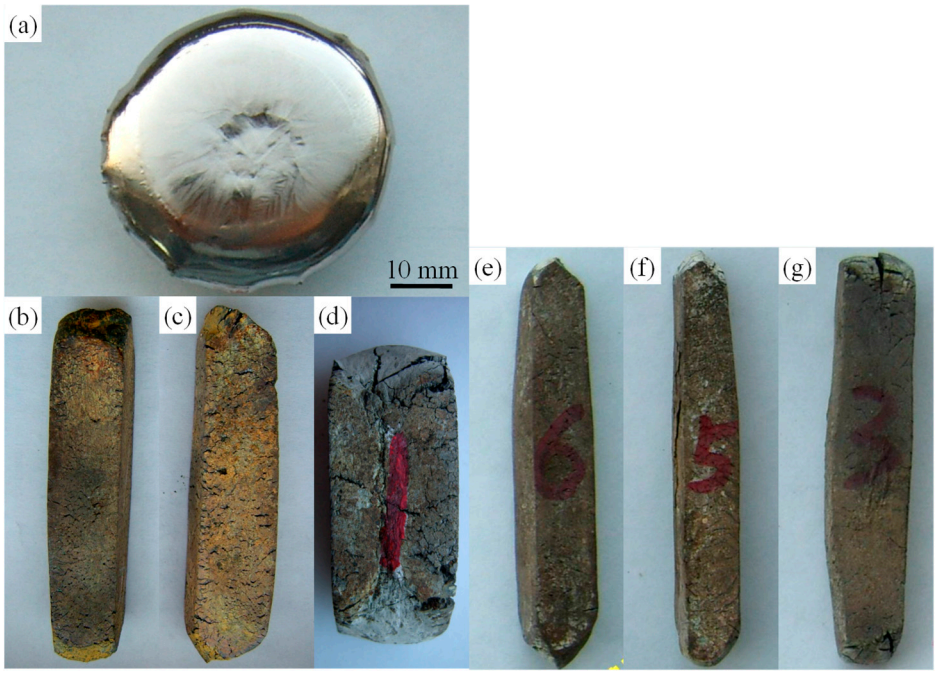

Figure 1. The morphologies of the 60 g ingot (**a**) and open-forged specimens (**b**–**g**). (**a**) 60 g ingot; (**b**) 2Zr-4O alloy; (**c**) 2Zr-6O alloy; (**d**) 2Zr-10O alloy; (**e**) 0Zr-4O alloy; (**f**) 0Zr-6O alloy; (**g**) 0Zr-10O alloy.

3.2. Effects of O and Zr on Microstructures

After solution treatment at 1010 °C for 30 min followed by water quenching, the microstructure of the 2Zr-1.2O alloy was equiaxed with the average grain size of approximately 200 μm (Figure 2a). After compression it is conceivable that the β grains changed into disk-like shapes, which were segmented by a mass of dislocations, stress-induced

α″ martensite and ω phase, {332}<113>β and {112}<111>β twins, kink bands, as well as shear bands [41]. In Ti alloys, O works as a β-stabilizer in the process of quenching in metastable β titanium alloys [24,39,46,51], while it works as an α-stabilizer during β/α phase transformation [52] and increases β transus dramatically, as shown in Table 1. In the other six alloys with higher O content, the elements redistributed and a short club-shaped α phase precipitated from the β matrix during furnace cooling, as shown in Figure 2d–i. All microstructures were taken from the central parts of the square bars. For 2Zr-10O and 0Zr-10O alloys, β transus are ~1234 °C and ~1264 °C, respectively. Because of extremely high β transus the solution temperature (1050 °C) for both alloys located in α + β phase field, and α phase grew up during solution and following furnace cooling. For 2Zr-4O, 2Zr-6O, 0Zr-4O and 0Zr-6O alloys, the solution temperatures are all located in β phase field, and α phase precipitated and grew up only during furnace cooling. Therefore, it can be observed that α phase in 2Zr-10O and 0Zr-10O alloys are larger than that in others. During heat treatment, the alloying elements will segregate, i.e., α-stabilizers segregate into α phase and β-stabilizers segregate into β phase. 2Zr-10O alloy was chosen to illustrate such changes Distribution of elements in 2Zr-10O alloy has been analyzed using EPMA. It clearly shows that conventional β-stabilizers, Nb and Ta, enriched in β phase matrix, conventional α-stabilizer, O, enriched in α phase, and Zr distributed uniformly in α and β phases, as shown in Figure 3.

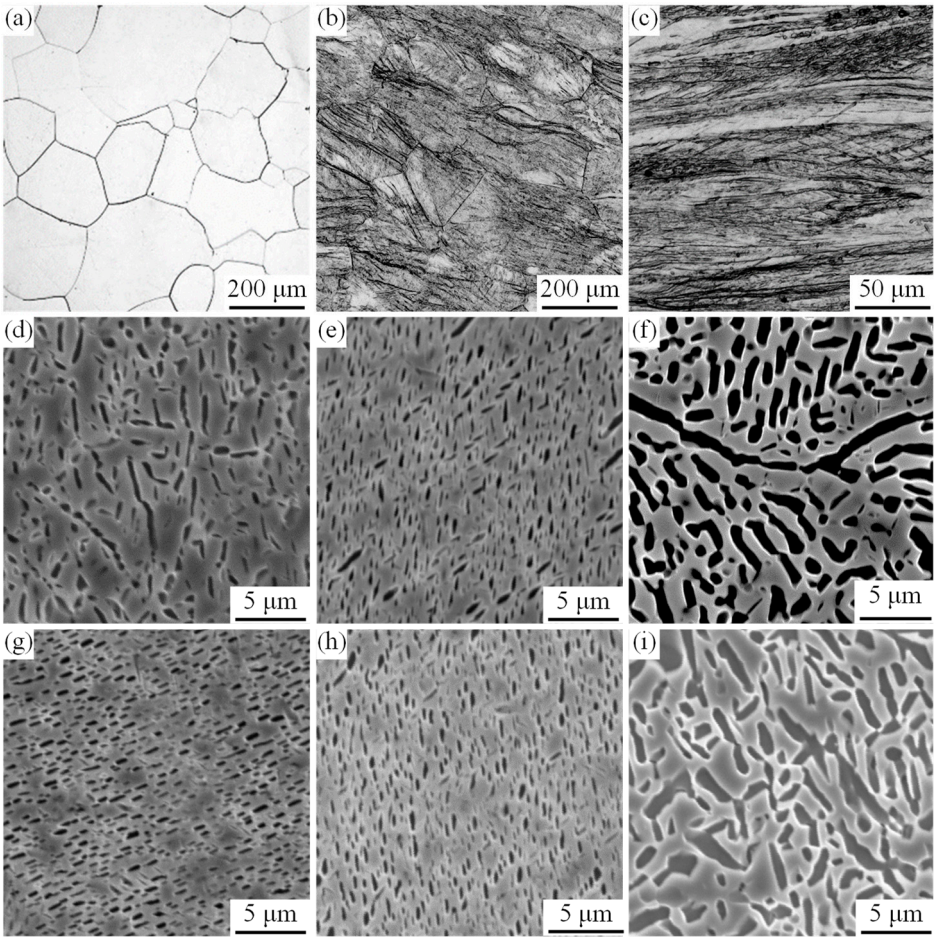

Figure 2. Microstructures of the alloys: (**a**) 2Zr-1.2O alloy after solution treatment; (**b**,**c**) 2Zr-1.2O alloy after cold compression, the observed plane is vertical (**b**) and parallel (**c**) to the compression direction; (**d**) 2Zr-4O alloy; (**e**) 2Zr-6O alloy; (**f**) 2Zr-10O alloy; (**g**) 0Zr-4O alloy; (**h**) 0Zr-6O alloy; (**i**) 0Zr-10O alloy.

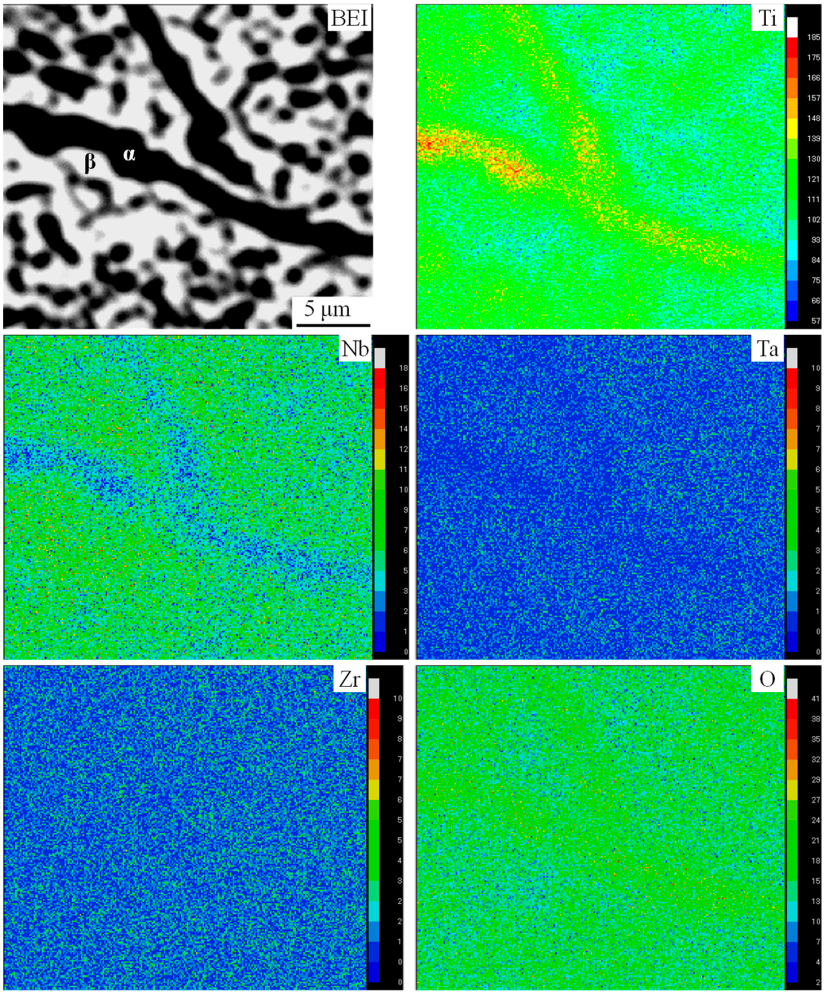

Figure 3. Distribution of elements in 2Zr-10O alloy.

XRD profiles of 2Zr-4O, 2Zr-6O and 2Zr-10O alloys are presented in Figure 4. It confirmed that the alloys contained α and β phases.

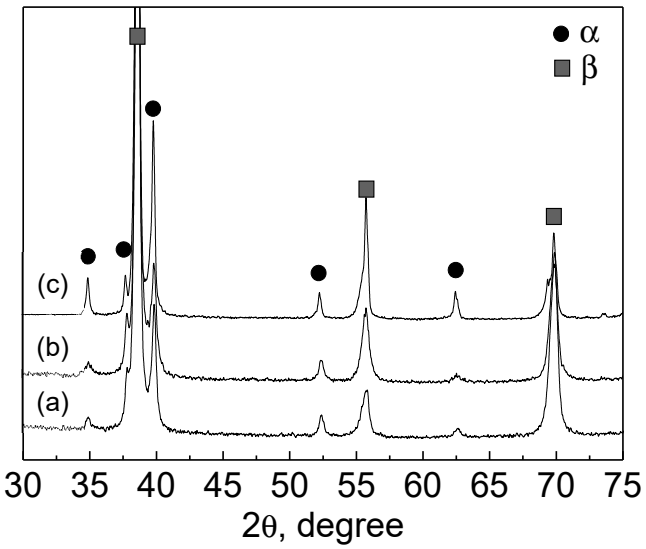

Figure 4. XRD profiles of the alloys after heat treatment: (**a**) 2Zr-4O alloy; (**b**) 2Zr-6O alloy; (**c**) 2Zr-10O alloy.

3.3. Effect of Temperature on Tensile Properties of 2Zr-1.2O Alloy

The tensile properties of cold-compressed 2Zr-1.2O alloy were tested in a range of −196 °C to 750 °C. At −196 °C the alloy presents an ultra-high strength of ~1800 MPa and an acceptable ductility of ~6.5% elongation and ~21% area reduction, which makes the alloy have the potential to be used at low temperatures. As the temperature increases the tensile strength decreases and the ductility increases, as shown in Figure 5. At 750 °C the alloy shows a tensile superplasticity with an elongation of ~168%, which may be related to the recrystallization of cold deformed microstructure. Figure 6 shows the specimens before and after the tensile test at 750 °C. It presents a high uniform elongation. The tensile fracture surfaces were observed under SEM, as shown in Figure 7. It can be found that the fracture surfaces at −196 °C and 19 °C have a similar fine dimple morphology, which means a typical ductile fracture. The fracture surface at 250 °C presents an entirely different morphology. It shows a large deep dimple morphology, which is formed via the combination of neighboring fine dimples. For the specimen at 750 °C, because of large elongation and area reduction, the fracture surface shows a fiber-like morphology.

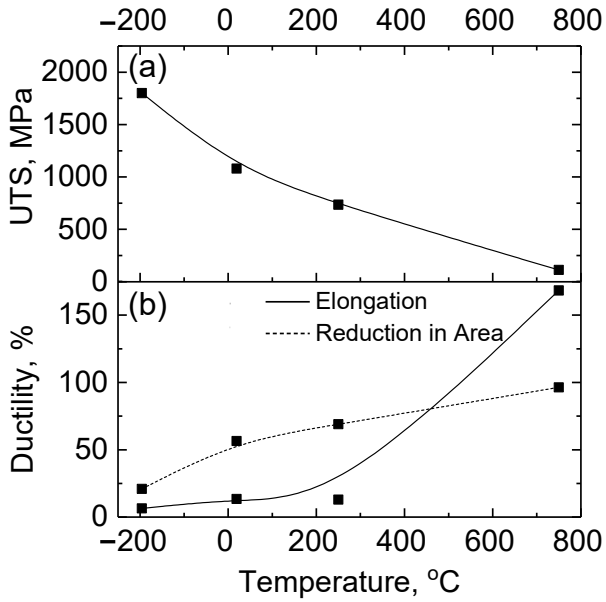

Figure 5. Tensile property of cold-compressed 2Zr-1.2O alloy: (**a**) Ultimate tensile strength (UTS) and (**b**) tensile ductility.

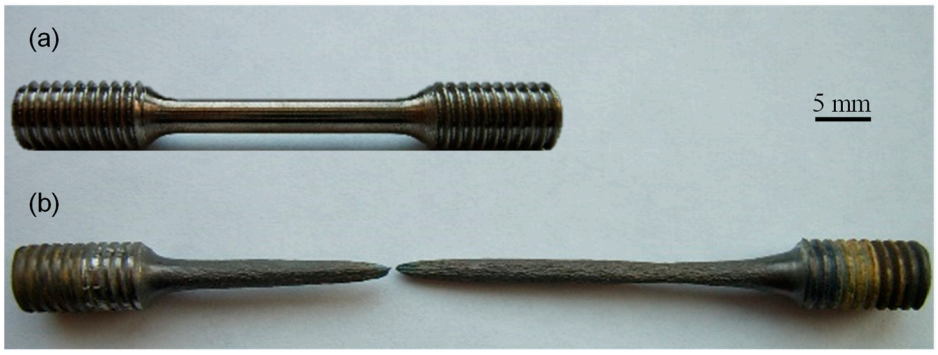

Figure 6. The 2Zr-1.2O alloy specimen before (**a**) and after (**b**) tensile test at 750 °C.

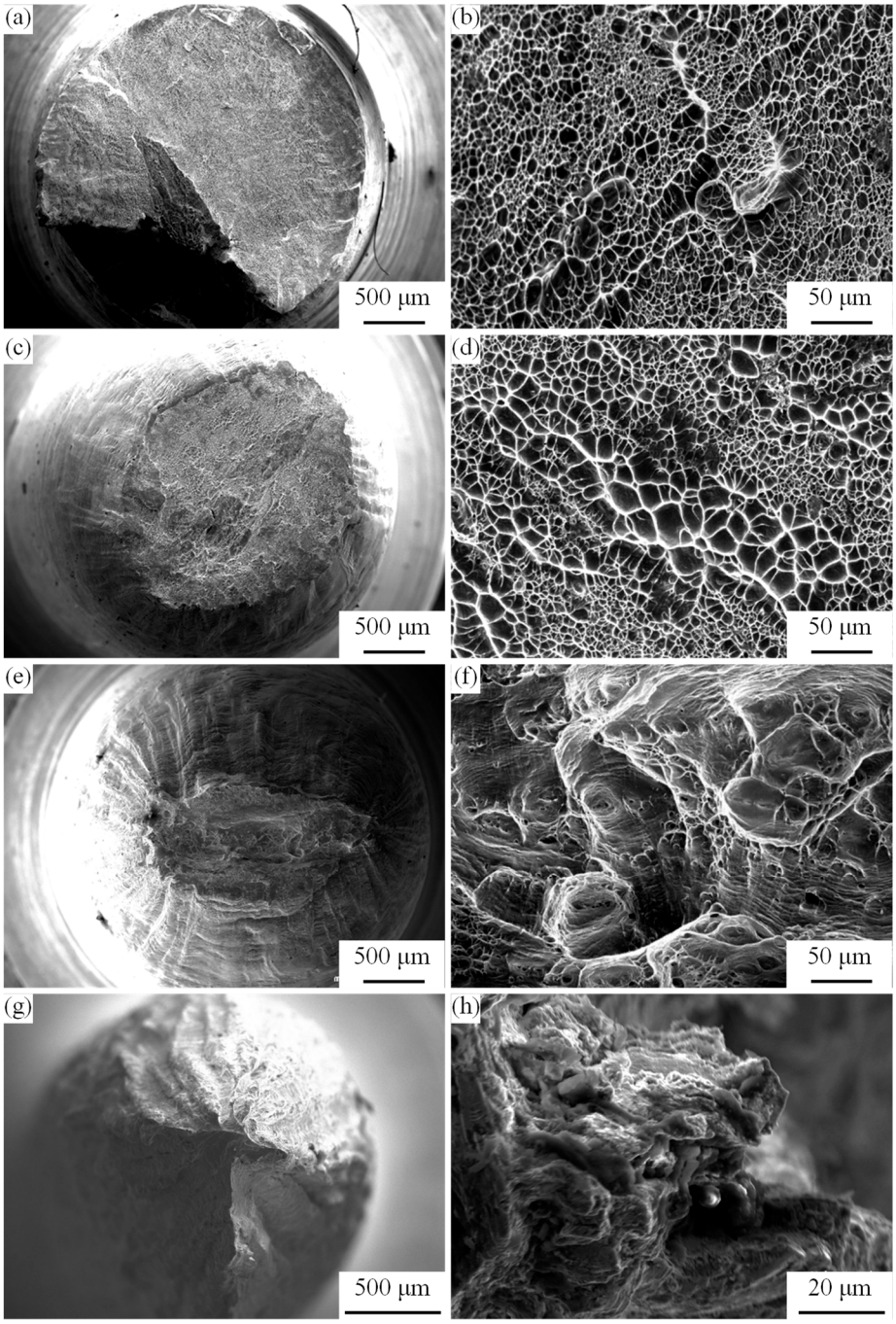

Figure 7. SEM images of the tensile fracture surfaces of 2Zr-1.2O alloy at different temperatures: (**a**,**b**) −196 °C; (**c**,**d**) 19 °C; (**e**,**f**) 250 °C; (**g**,**h**) 750 °C. (**a**,**c**,**e**,**g**) The entire fracture surfaces; (**b**,**d**,**f**,**h**) the enlarged images of fracture surfaces.

3.4. Effects of O and Zr on Mechanical Properties

Hardness is one of the most important mechanical properties of the alloy. It can be used to evaluate the strength changing conveniently and simply. In the present study, Vickers-hardnesses (HV) of the alloys at room temperature were tested and the results were shown in Figure 8a. It shows that as O content increases the HV increases dramatically, and the Zr-containing alloys have a higher HV. For 2Zr-xO alloys when the O content increases from 4% to 10% HV increases from 2.94 GPa to 4.40 GPa. For 0Zr-xO alloys when the O

content increases from 4% to 10% HV increases from 2.62 GPa to 3.85 GPa. The relationship between O content and HV can be expressed as:

$$HV_{2Zr} = 1.96 + 0.24[O], \quad (1)$$

$$HV_{0Zr} = 1.79 + 0.21[O], \quad (2)$$

where [O] is oxygen content in at.%, Equation (1) is for 2Zr-xO alloys and Equation (2) is for 0Zr-xO alloys.

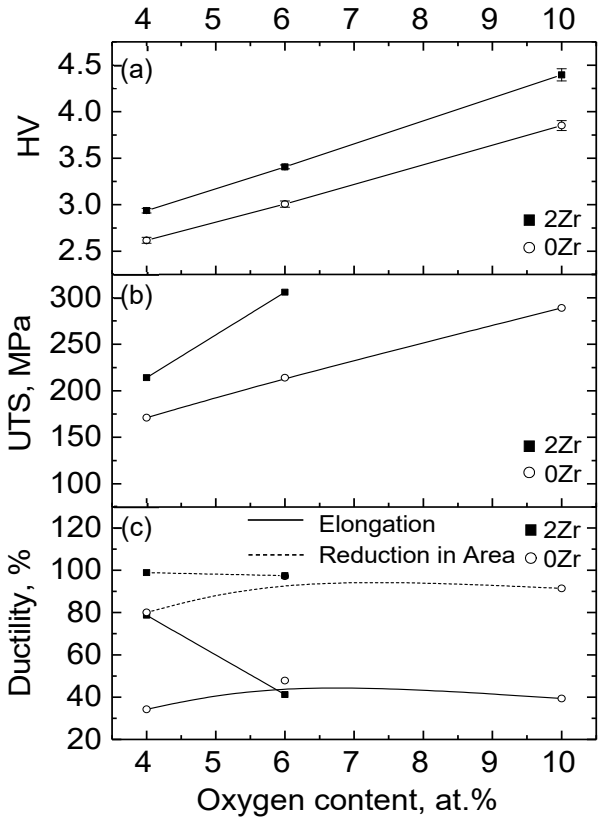

Figure 8. Effect of oxygen and zirconium contents on the mechanical properties: (**a**) Vickers-hardness (HV) at room temperature; (**b**) Ultimate tensile strength (UTS) and (**c**) tensile ductility at 750 °C.

This means that HV will be increased by ~0.24 GPa on average for 2Zr-xO alloys and ~0.21 GPa on average for 0Zr-xO alloys as O content is increased by 1%. It indicates that Zr addition increases the strengthening effect of O.

The effects of O and Zr on ultimate tensile strength (UTS) at 750 °C shows a similar trend, as shown in Figure 8b. O increases the strength dramatically. It is similar to that at lower temperatures [13,31,33,46]. The solution strengthening effect of O is obvious even at 750 °C. In the Zr-containing alloys, the strengthening effect of O is more intensive. The relationship between O content and UTS can be expressed as:

$$UTS_{2Zr} = 30.00 + 46.00[O], \quad (3)$$

$$UTS_{0Zr} = 94.43 + 19.54[O], \quad (4)$$

where [O] is oxygen content in at.%, Equation (3) is for 2Zr-xO alloys and Equation (4) is for 0Zr-xO alloys.

All of the alloys exhibited perfect ductility at 750 °C with the elongation above 34% and reductions in area above 80%. Compared with at room temperature [20], the negative effect of O on the plasticity reduces at elevated temperature.

The tensile fracture surfaces were shown in Figures 9 and 10. For 2Zr-4O and 2Zr-6O alloys large deep dimple morphology are observed. For Zr-free alloys, the size of dimples is finer. All alloys present typical ductile fractures.

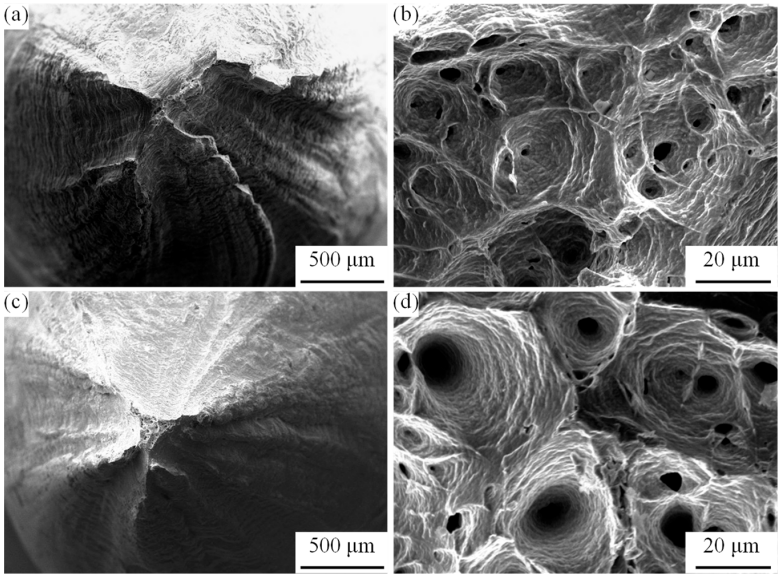

Figure 9. SEM images of the tensile fracture surfaces of the alloys at 750 °C: (**a**,**b**) 2Zr-4O alloy; (**c**,**d**) 2Zr-6O alloy. (**a**,**c**) The entire fracture surfaces; (**b**,**d**) the enlarged images of fracture surfaces.

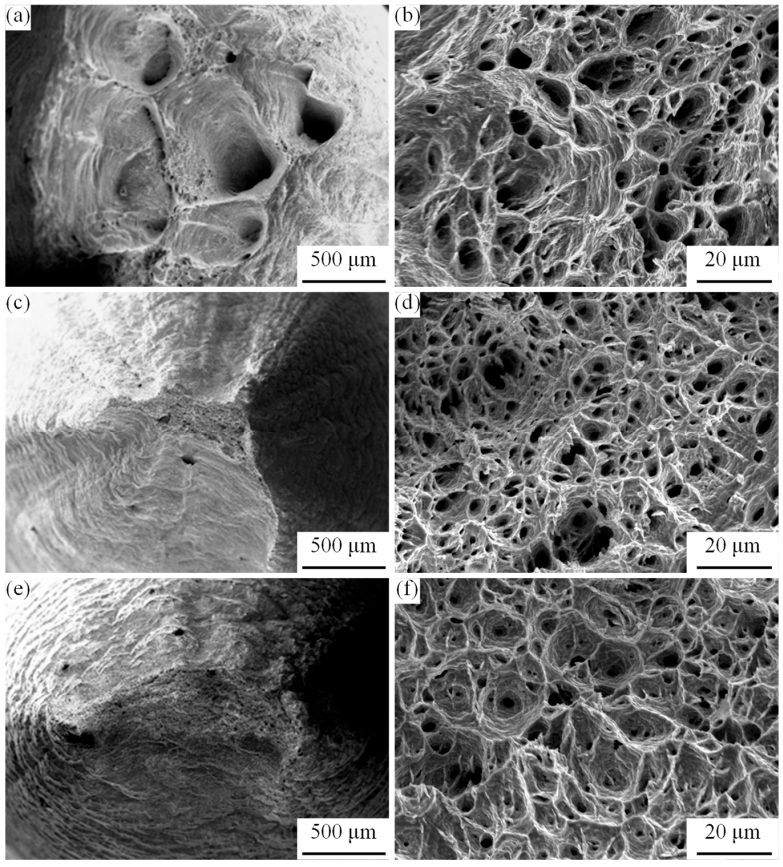

Figure 10. SEM images of the tensile fracture surfaces of the alloys at 750 °C: (**a**,**b**) 0Zr-4O alloy; (**c**,**d**) 0Zr-6O alloy; (**e**,**f**) 0Zr-10O alloy. (**a**,**c**,**e**) The entire fracture surfaces; (**b**,**d**,**f**) the enlarged images of fracture surfaces.

4. Discussion

A few works have been done about the effects of N or O on the mechanical properties of β titanium alloys. Furuhara et al. [25], Hou et al. [26], Kim et al. [24], Qazi et al. [29] and Furuta et al. [46] have studied the tensile properties of Ti-10V-2Fe-3V-(0.009–0.2)N (wt.%), Ti-30Nb-12Zr-(0.08–0.5)O(-(0.09–0.49)N) (wt.%), Ti-22Nb-(0–2)O (mol.%), Ti-35Nb-7Zr-5Ta-(0.06–0.68)O (wt.%) and Ti-36Nb-2Ta-3Zr-(0.07–0.93)O (wt.%) alloys, respectively. Almost all the results showed that O or N increased the tensile strength and decreased the ductility. Moreover, the N or O could improve the elasticity of the alloys [25,27,46]. In the low-alloyed titanium alloys, in which the dominant phase is the α phase, the effect of O content on the tensile properties also showed similar results to those mentioned above. The relationship between HV of α titanium alloy and N or O content was given by the equation of $HV = a + b[O(N)]^{1/2}$ [20,53], where the exponent is 1/2 rather than 1 in the present study. This indicates that the effect of O on the HV and UTS in the present study is more significant than that in the α titanium alloy. Especially the increasing rates of HV and UTS along with O content in the 2Zr-xO alloys are more rapid than those in the 0Zr-xO alloys. Duplex phases in the studied alloys cause a compound strengthening effect. At the same time, the effects of Zr and O on the strength interact with each other. Zr enhances the strengthening effect of O and Zr has a better strengthening effect in the condition of higher O content. This may be induced by the formation of the Zr-O atom clusters, which could effectively inhibit dislocation activity and produce an improved strengthening effect in the present alloy system [30].

In the above analysis, the effects of the size of the α phase on the HV at room temperature and tensile strength at 750 °C were ignored. Xu's research [54] indicated that a precipitated phase with a size beyond about 0.4 μm had a very small precipitation strengthening effect. In (0, 2)Zr-4O, (0, 2)Zr-6O and (0, 2)Zr-10O alloys, the widths of the α phase are all above 0.5 μm. Therefore, it is reasonable to simplify the discussions. The morphologies of the micro-fractures (Figures 9 and 10) also provide some evidence. The characteristics of micro-fractures of these five alloys are only related to the Zr content. The Zr-containing alloys show big nest-like dimple morphology (Figure 9b,d), and the Zr-free alloys show fine dimple morphology (Figure 10b,d,f), although the size of α phase in (0, 2)Zr-10O alloys is much bigger than that in other alloys.

5. Conclusions

Ti-23Nb-0.7Ta-(0, 2)Zr-(1.2, 4, 6, 10)O alloys were prepared using a non-consumable arc-melting method and open-forged at elevated temperature. The effects of O and Zr on the thermal forgeability were estimated. Ti-23Nb-0.7Ta-2Zr-1.2O alloy was tensed at a temperature range of −196 °C to 750 °C. The influence of O and Zr contents on room-temperature hardness and tensile property at 750 °C were investigated. The following conclusions can be drawn:

(1) Ti-23Nb-0.7Ta-2Zr-1.2O alloy shows wonderful forgeability. Along with the O content increasing, the thermal forgeability of the alloys decreases. Zr has a negative effect on thermal forgeability.

(2) For Ti-23Nb-0.7Ta-2Zr-1.2O alloy, the UTS decreases, and the ductility increases with the temperature increasing. At 750 °C the alloy shows a tensile superplasticity with an elongation of ~168%.

(3) All of the alloys exhibit perfect ductility at 750 °C with the elongation above 34% and reductions in area above 80%. Room-temperature HV and 750 °C UTS increase as O and Zr contents increase. HV will be increased by ~0.24 GPa on average for 2Zr-xO alloys and ~0.21 GPa on average for 0Zr-xO alloys as O content is increased 1%. UTS will be increased ~46.00 MPa on average for 2Zr-xO alloys and ~19.54 MPa on average for 0Zr-xO alloys as O content is increased by 1%. Zr enhances the strengthening effect of O and Zr has better strengthening effects in the condition of higher O content.

Author Contributions: Writing—original draft preparation, K.S.; validation, X.W.; investigation, Z.Y.; resources, S.W.; writing—review and editing, G.L.; supervision, Y.Y. and K.Z.; project administration, H.W. and A.H. All authors have read and agreed to the published version of the manuscript.

Funding: This research was funded by Natural Science Foundation of Shanghai (grant No. 21ZR1445100) and Major Special Science and Technology Project of Yunnan Province (grant No. 202002AB080001-3).

Institutional Review Board Statement: Not applicable.

Informed Consent Statement: Not applicable.

Data Availability Statement: The data presented in this study are available on request from the corresponding author.

Conflicts of Interest: The authors declare no conflict of interest.

References

1. Williams, J.C.; Starke, E.A. Progress in structural materials for aerospace systems. *Acta Mater.* **2003**, *51*, 5775–5799. [CrossRef]
2. Rack, H.J.; Qazi, J.I. Titanium alloys for biomedical applications. *Mater. Sci. Eng. C* **2006**, *26*, 1269–1277. [CrossRef]
3. Niinomi, M. Recent research and development in titanium alloys for biomedical applications and healthcare goods. *Sci. Technol. Adv. Mat.* **2003**, *4*, 445–454. [CrossRef]
4. Boyer, R. Titanium Airframe Applications: Brief History, Present Applications and Future Trends. *Mater. Sci. Forum.* **2003**, *426–432*, 643–648. [CrossRef]
5. Bania, P.J. Next generation titanium alloys for elevated temperature service. *ISIJ Int.* **1991**, *31*, 840–847. [CrossRef]
6. Walker, I.R. Considerations on the selection of alloys for use in pressure cells at low temperatures. *Cryogenics* **2005**, *45*, 87–108. [CrossRef]
7. Zhou, Y.L.; Niinomi, M.; Akahori, T. Effects of Ta content on Young's modulus and tensile properties of binary Ti–Ta alloys for biomedical applications. *Mater. Sci. Eng. A* **2004**, *371*, 283–290. [CrossRef]
8. Masumoto, K.; Horiuchi, Y.; Inamura, T.; Hosoda, H.; Wakashima, K.; Kim, H.Y.; Miyazaki, S. Effects of Si addition on superelastic properties of Ti–Nb–Al biomedical shape memory alloys. *Mater. Sci. Eng. A* **2006**, *438–440*, 835–838. [CrossRef]
9. Lutjering, G. Influence of processing on microstructure and mechanical properties of (α + β) titanium alloys. *Mater. Sci. Eng. A* **1998**, *243*, 32–45. [CrossRef]
10. Kawabe, Y.; Muneki, S. Strengthening and Toughening of Titanium Alloys. *ISIJ Int.* **1991**, *31*, 785–791. [CrossRef]
11. Martin, P.L. Effects of hot working on the microstructure of Ti-base alloys. *Mater. Sci. Eng. A* **1998**, *243*, 25–31. [CrossRef]
12. Lutjering, G. Property optimization through microstructural control in titanium and aluminum alloys. *Mater. Sci. Eng. A* **1999**, *263*, 117–126. [CrossRef]
13. Varlioglu, M.; Nash, P.; Xu, F.; Li, G.P. The effect of increased zirconium content on the microstructure and mechanical properties of Ti-1100 alloy. *Light Met. Age* **2004**, *62*, 32–35.
14. Shimagami, K.; Ito, T.; Toda, Y.; Yumoto, A.; Yamabe-Mitarai, Y. Effects of Zr and Si addition on high-temperature mechanical properties and microstructure in Ti-10Al-2Nb-based alloys. *Mater. Sci. Eng. A* **2019**, *756*, 46–53. [CrossRef]
15. Jiao, Z.; Ma, C.; Fu, J.; Cheng, X.; Tang, H.; Liu, D.; Zhang, J. The effects of Zr contents on microstructure and properties of laser additive manufactured Ti-6.5Al-3.5Mo-0.3Si-xZr alloys. *J. Alloy. Compd.* **2018**, *745*, 592–598. [CrossRef]
16. Jing, R.; Liang, S.X.; Liu, C.Y.; Ma, M.Z.; Zhang, X.Y.; Liu, R.P. Structure and mechanical properties of Ti–6Al–4V alloy after zirconium addition. *Mater. Sci. Eng. A* **2012**, *552*, 295–300. [CrossRef]
17. Huang, C.; Zhao, Y.; Xin, S.; Zhou, W.; Li, Q.; Zeng, W. Effect of microstructure on tensile properties of Ti–5Al–5Mo–5V–3Cr–1Zr alloy. *J. Alloy. Compd.* **2017**, *693*, 582–591. [CrossRef]
18. Zhou, Y.; Li, Y.; Yang, X.; Cui, Z.; Zhu, S. Influence of Zr content on phase transformation, microstructure and mechanical properties of $Ti_{75-x}Nb_{25}Zr_x$ (x = 0–6) alloys. *J. Alloy. Compd.* **2009**, *486*, 628–632. [CrossRef]
19. Ba, H.; Dong, L.; Zhang, Z.; Xu, D.; Yang, R. Effects of Zr Content on the Microstructures and Tensile Properties of Ti–3Al–8V–6Cr–4Mo–xZr Alloys. *Acta. Metall. Sin. Engl. Lett.* **2016**, *29*, 722–726. [CrossRef]
20. Zhang, X.Y.; Zhao, Y.Q.; Bai, C.G. *Titanium Alloys and Their Applications*, 3rd ed.; Chemical Industry Press: Beijing, China, 2005; p. 60.
21. Abdel-Hady, M.; Fuwa, H.; Hinoshita, K.; Kimura, H.; Shinzato, Y.; Morinaga, M. Phase stability change with Zr content in β-type Ti–Nb alloys. *Scr. Mater.* **2007**, *57*, 1000–1003. [CrossRef]
22. Min, X.H.; Emura, S.; Zhang, L.; Tsuzaki, K. Effect of Fe and Zr additions on ω phase formation in β-type Ti–Mo alloys. *Mater. Sci. Eng. A* **2008**, *497*, 74–78. [CrossRef]
23. Ikeda, M.; Komatsu, S.-Y.; Nakamura, Y. Effects of Sn and Zr additions on phase constitution and aging behavior of Ti-50 mass%Ta alloys quenched from β single phase region. *Mater. Trans.* **2004**, *45*, 1106–1112. [CrossRef]

24. Kim, J.I.; Kim, H.Y.; Hosoda, H.; Miyazaki, S. Shape memory behavior of Ti-22Nb-(0.5–2.0)O(at%) biomedical alloys. *Mater. Trans.* **2005**, *46*, 852–857. [CrossRef]
25. Furuhara, T.; Annaka, S.; Tomio, Y.; Maki, T. Superelasticity in Ti–10V–2Fe–3Al alloys with nitrogen addition. *Mater. Sci. Eng. A* **2006**, *438–440*, 825–829. [CrossRef]
26. Hou, F.Q.; Li, S.J.; Hao, Y.L.; Yang, R. Nonlinear elastic deformation behaviour of Ti–30Nb–12Zr alloys. *Scr. Mater.* **2010**, *63*, 54–57. [CrossRef]
27. Li, S.J.; Jia, M.T.; Prima, F.; Hao, Y.L.; Yang, R. Improvements in nonlinear elasticity and strength by grain refinement in a titanium alloy with high oxygen content. *Scr. Mater.* **2011**, *64*, 1015–1018. [CrossRef]
28. Qazi, J.I.; Marquardt, B.; Allard, L.F.; Rack, H.J. Phase transformations in Ti–35Nb–7Zr–5Ta–(0.06–0.68)O alloys. *Mater. Sci. Eng. C* **2005**, *25*, 389–397. [CrossRef]
29. Qazi, J.I.; Tsakiris, V.; Marquardt, B.; Rack, H.J. *Effect of Aging Treatments on the Tensile Properties of Ti-35Nb-7Zr-5Ta-(0.06–0.7)O Alloys*; ASTM International: West Conshohocken, PA, USA, 2005; Volume 2.
30. Saito, T.; Furuta, T.; Hwang, J.H.; Kuramoto, S.; Nishino, K.; Suzuki, N.; Chen, R.; Yamada, A.; Ito, K.; Seno, Y.; et al. Multifunctional alloys obtained via a dislocation-free plastic deformation mechanism. *Science* **2003**, *300*, 464–467.
31. Furuta, T.; Nishino, K.; Hwang, J.H.; Yamada, A.; Ito, K.; Osawa, S.; Kuramoto, S.; Suzuki, N.; Chen, R.; Saito, T. Development of multi functional titanium alloy, "GUM METAL", Ti-2003 Science and Technology. In Proceedings of the 10th World Conference on Titanium, Hamburg, Germany, 13 July 2003.
32. Gutkin, M.Y.; Ishizaki, T.; Kuramoto, S.; Ovid'ko, I.A. Nanodisturbances in deformed Gum Metal. *Acta Mater.* **2006**, *54*, 2489–2499. [CrossRef]
33. Saito, T.; Furuta, T.; Hwang, J.H.; Kuramoto, S.; Nishino, K.; Suzuki, N.; Chen, R.; Yamada, A.; Ito, K.; Seno, Y.; et al. Multi Functional Titanium Alloy "GUM METAL". *Mater. Sci. Forum.* **2003**, *426–432*, 681–688. [CrossRef]
34. Kuramoto, S.; Furuta, T.; Hwang, J.; Nishino, K.; Saito, T. Elastic properties of Gum Metal. *Mater. Sci. Eng. A* **2006**, *442*, 454–457. [CrossRef]
35. Kuramoto, S.; Furuta, T.; Hwang, J.H.; Nishino, K.; Saito, T. Plastic deformation in a multifunctional Ti-Nb-Ta-Zr-O alloy. *Metall. Mater. Trans. A* **2006**, *37*, 657–662. [CrossRef]
36. Ikehata, H.; Nagasako, N.; Kuramoto, S.; Saito, T. Designing new structural materials using density functional theory: The example of Gum Metal. *MRS Bull.* **2006**, *31*, 688–692. [CrossRef]
37. Li, T.; Morris, J.W., Jr.; Nagasako, N.; Kuramoto, S.; Chrzan, D.C. "Ideal" engineering alloys. *Phys. Rev. Lett.* **2007**, *98*, 105503. [CrossRef]
38. Yang, Y.; Li, G.P.; Cheng, G.M.; Li, Y.L.; Yang, K. Multiple deformation mechanisms of Ti–22.4Nb–0.73Ta–2.0Zr–1.34O alloy. *Appl. Phys. Lett.* **2009**, *94*, 061901. [CrossRef]
39. Yang, Y.; Li, G.P.; Cheng, G.M.; Wang, H.; Zhang, M.; Xu, F.; Yang, K. Stress-introduced α" martensite and twinning in a multifunctional titanium alloy. *Scr. Mater.* **2008**, *58*, 9–12. [CrossRef]
40. Yang, Y.; Li, G.P.; Wang, H.; Wu, S.Q.; Zhang, L.C.; Li, Y.L.; Yang, K. Formation of zigzag-shaped {112}<111>β mechanical twins in Ti–24.5 Nb–0.7 Ta–2 Zr–1.4 O alloy. *Scr. Mater.* **2012**, *66*, 211–214. [CrossRef]
41. Yang, Y.; Wu, S.Q.; Li, G.P.; Li, Y.L.; Lu, Y.F.; Yang, K.; Ge, P. Evolution of deformation mechanisms of Ti–22.4Nb–0.73Ta–2Zr–1.34O alloy during straining. *Acta Mater.* **2010**, *58*, 2778–2787. [CrossRef]
42. Qu, L.; Yang, Y.; Lu, Y.F.; Feng, L.; Ju, J.H.; Ge, P.; Zhou, W.; Han, D.; Ping, D.H. A detwinning process of {332}<113> twins in beta titanium alloys. *Scr. Mater.* **2013**, *69*, 389–392. [CrossRef]
43. Xing, H.; Sun, J. Mechanical twinning and omega transition by <111>{112} shear in a metastable β titanium alloy. *Appl. Phys. Lett.* **2008**, *93*, 93–95. [CrossRef]
44. Talling, R.J.; Dashwood, R.J.; Jackson, M.; Dye, D. On the mechanism of superelasticity in Gum metal. *Acta Mater.* **2009**, *57*, 1188–1198. [CrossRef]
45. Talling, R.; Dashwood, R.; Jackson, M.; Kuramoto, S.; Dye, D. Determination of (C_{11}-C_{12}) in Ti–36Nb–2Ta–3Zr–0.3O (wt.%) (Gum metal). *Scr. Mater.* **2008**, *59*, 669–672. [CrossRef]
46. Furuta, T.; Kuramoto, S.; Rong, C.; Hwang, J.; Nishino, K.; Saito, T.; Ikeda, M. Effect of oxygen on phase stability and elastic deformation behavior in Gum Metal. *J. Jpn. Inst. Met.* **2006**, *70*, 579–585. [CrossRef]
47. Furuta, T.; Kuramoto, S.; Hwang, J.; Nishino, K.; Saito, T.; Niinomi, M. Mechanical Properties and Phase Stability of Ti-Nb-Ta-Zr-O Alloys. *Mater. Trans.* **2007**, *48*, 1124–1130. [CrossRef]
48. Besse, M.; Castany, P.; Gloriant, T. Mechanisms of deformation in gum metal TNTZ-O and TNTZ titanium alloys: A comparative study on the oxygen influence. *Acta Mater.* **2011**, *59*, 5982–5988. [CrossRef]
49. Wei, Q.; Wang, L.; Fu, Y.; Qin, J.; Lu, W.; Zhang, D. Influence of oxygen content on microstructure and mechanical properties of Ti–Nb–Ta–Zr alloy. *Mater. Des.* **2011**, *32*, 2934–2939. [CrossRef]
50. Sun, S.Y.; Deng, C. Accurate calculation of α + β/β phase transition of titanium alloys based on binary phase diagrams. *Titan. Ind. Prog.* **2011**, *28*, 21–25.
51. Abdel-Hady, M.; Hinoshita, K.; Morinaga, M. General approach to phase stability and elastic properties of β-type Ti-alloys using electronic parameters. *Scr. Mater.* **2006**, *55*, 477–480. [CrossRef]

52. Lütjering, G.; Williams, J.C. *Titanium*, 2nd ed.; Springer: Berlin, Germany, 2007; p. 46.
53. Ando, T.; Nakashima, K.; Tsuchiyama, T.; Takaki, S. Microstructure and mechanical properties of a high nitrogen titanium alloy. *Mater. Sci. Eng. A* **2008**, *486*, 228–234. [CrossRef]
54. Xu, F. The Effect of Zr Addition on 650 °C Deformation and Fracture Mechanisms in Ti-1100 Alloy. Ph.D. Thesis, Chinese Academy of Sciences, Shenyang, China, 2007.